Photoacoustics 8 (2017) 1–7

Contents lists available at ScienceDirect

Photoacoustics

journal homepage: www.elsevier.com/locate/pacs

Research articles

Visualization of photoacoustic images in a limited-View measuring system using eigenvalues of a photoacoustic transmission matrix

Hiroshi Abe*, Tsuyoshi Shiina

Graduate school of medicine, Kyoto University Kyoto, Japan

ARTICLE INFO

Article history:
Received 22 December 2016
Received in revised form 15 June 2017
Accepted 21 June 2017
Available online 1 July 2017

ABSTRACT

Photoacoustic imaging is a unique imaging method that involves extracting information from points at different depths, an advantage of ultrasound imaging, while maintaining functional information, a key feature of conventional photo imaging. This makes it easy to add functional images to ultrasound images by adding a laser pulse source to the conventional ultrasound imaging device and detecting a photo-ultrasound signal via a conventional ultrasound probe. One challenge when using normal one-dimensional (1D) probes and generating photoacoustic images is the limited-view problem, in which artefacts are observed due to the positions of the ultrasound transducers. In this study, we used a photoacoustic transmission matrix (PA-TM) for simulation and performed a verification test using a 1D probe and a phantom. The results confirmed that the eigenvalues of the PA-TM visualized the light absorber itself in the limited-view measurement system, which eliminates reconstruction artefacts and further scattering artefacts, and that visualization is possible by signal intensity amplification through further phase modulation.

1. Introduction

Photoacoustic tomography is an emerging non-invasive hybrid light and ultrasound imaging technique. Illuminating an object with uniform short-pulse laser light leads to thermoelastic expansion at sites of optical absorption. Generated photoacoustic ultrasound waves can be measured using an ultrasound transducer and then reconstructed based on the straightness of the ultrasound wave. Light can provide a functional, metabolic, and molecular contrast signal. However, the ultrasound transducer cannot determine the source of the generated photoacoustic signal, due to diffusion of light in the object. Consequently, ultrasound transducers must be placed in multiple locations around the object to avoid omission of image information. In many practical implementations, ultrasound transducers are placed over an aperture that does not enclose the object, and the result is the limited-view problem [1]. To avoid this problem, arc-shaped and bowl-shaped transducers are employed instead of the generally used 1D ultrasound transducers [2,3]. With ultrasound imaging, the transmitted ultrasound does not have functional interaction with the object; however, with a beam-forming technique, a complex set of control pulses emitted from 1D ultrasound transducers can form arc-shaped sound waves, resulting in a high-quality image.

Several techniques have been proposed to localize the area emitting the photoacoustic signal. The first technique is based on localized vibration tagging at the absorption areas. Induced by the acoustic radiation force in a focused ultrasonic beam, signals of interest can be distinguished by tagging the photoacoustic signal at the origin using localized tissue vibration [4]. This technique can eliminate the clutter signal; however, it is necessary to scan all image areas with a high-energy ARF beam and to acquire photoacoustic signals sequentially.

The second technique is to control the scattering light by combining optical phase conjugation and ultrasound tagging. Ultrasound is used to define a target modulation location, and a phase conjugating mirror (PCM) is used to return time-reversing tagging light to the ultrasound modulation location. Analog [5] and digital [6,7] approaches have been used to create a PCM. With the analog approach, photorefractive crystals are used to record the phase hologram and replay the time-reversing light holographically. Although these crystals have high sensitivity for recording phase holograms, the readout light has higher gain than the recording light and erases the photorefractive holograms. With the digital approach, an interference fringe is captured using a digital

* Corresponding author.
E-mail addresses: abe.hiroshi.53v@st.kyoto-u.ac.jp (H. Abe), shiina.tsuyoshi.6w@kyoto-u.ac.jp (T. Shiina).

http://dx.doi.org/10.1016/j.pacs.2017.06.003

camera, and the phase hologram is calculated. The phase holograms are subsequently projected onto the spatial light modulator (SLM), and the readout light replays the time-reversing light. These principles are highly elegant, but the system requires accurate alignment [8] and repeated iterative focusing to achieve high gain [9]. Because focusing enhancement is greatly restricted by the size of the focusing area, it is unsuitable for the illumination used for tomography.

The third technique is optical wavefront shaping [10,11]. Using a feedback photoacoustic signal from the target location related to light energy, incident light is optimized using a wavefront control device with an iterative optimization algorithm [12].

Another important technique involves using the photoacoustic transmission matrix (PA-TM). This approach uses the transmission matrix to detect, localize, and selectively focus light on light-absorbing targets through diffusive samples for a photoacoustic system with a single transducer [13], and is based on the coherence of the laser light. However, acquiring the photoacoustic signal observed as a point light source causes a local photoacoustic effect, and the emitted photoacoustic signal can be detected by a 1D transducer as a point spread propagated wave [14]. This technique eliminates reconstruction artefacts. By combining these two techniques, it is possible to derive the PA-TM using a 1D transducer [15].

In this study, we focus on the singular value following derivation of the PA-TM and propose a technique for visualization of the light response distribution and suppression of the reconstruction artefact under a limited-view measurement system. This enables determination of both the presence of light absorbers and the degree of control of the localized light quantity with high contrast by compressing the artefact.

2. Theory

2.1. Photoacoustic transmission matrix

As laser light enters a scatterer, each of the wavefronts (i = 1, 2, . . . , n) is scattered inside the scatterer and then emitted from its surfaces (j = 1, 2, . . . , m) in a random-phase state (Fig. 1(a)). Therefore, if the phase state of the light at each location is uniform, the state of the light at the emitting surface can be expressed as $|t_{ij}|e^{\phi_{ij}}$, which includes a random phase component. In such conditions, observing the surface using a camera reveals a speckle of light particles, which means that light interference occurs at each surface. The light can be modulated if it is possible to modulate the phase of the incident light and cause interference, and to calculate the transmission matrix that expresses the light's response. For coherent light, speckle intensity can be adjusted by modulating the phase at the incident surface. Light can be focused by setting the light source in such a manner that light rays passing through the observed surface are in phase (Fig. 1(b)). It is also possible to create dark spaces using peripheral brightness.

In general, light loses its straightness after travelling a scattering distance longer than the mean free path; for example, it is impossible to observe the phase status inside a living substance, the scatterer, using a camera that captures light intensity. However, if light-absorbing substances are present in the scatterer, a photoacoustic phenomenon is induced by the change in energy associated with light absorption, and it is possible to detect a photoacoustic wave signal, which is proportional to the energy of the absorbed light. Moreover, various reconstruction methods have been proposed based on the transmission time and straightness of an ultrasound signal, which enables identification of the location of the light-absorbing substance. Therefore, it is possible to calculate the response matrix for the light at the light-absorbing substance by modulating the phase of the incident light. We used a light response rate corresponding to a singular value of the response matrix at each position of the light-absorbing substance, and attempted to visualize the light-absorbing substances inside a scatterer.

Furthermore, the photoacoustic wave generated by light irradiation in each pattern is measured using the coherence status of the light; thus, the irradiation has a speckled pattern. Therefore, the photoacoustic wave has essentially an N-type waveform and forms a composite wavefront along its shape. With this irradiation method, the photoacoustic wave is formed from speckle points and propagates [14,15]. Therefore, it is possible to detect signals without the limited-view problem that arises with measurement using a photoacoustic 1D array transducer. In the actual measurement system, however, complete reconstruction is not possible, due to restrictions in aperture and bandwidth arising from the finite diameter of the transducer, and image artefacts are generated during the reconstruction. In the phase measurement, the offset is cancelled and the information is extracted from the phase response, which is not hampered by the artefacts.

2.2. Measurement of the PA-TM eigenvalue

We used the Hadamard matrix to modulate the phase of each input wavefront (Fig. 2(a)). The Hadamard matrix is a square matrix composed of −1 and 1, with π or 0 as the phase. To observe the output status, we used the periphery of the phase-modulating device as the reference phase plane, since interference measurements were taken to obtain the response to the input phase.

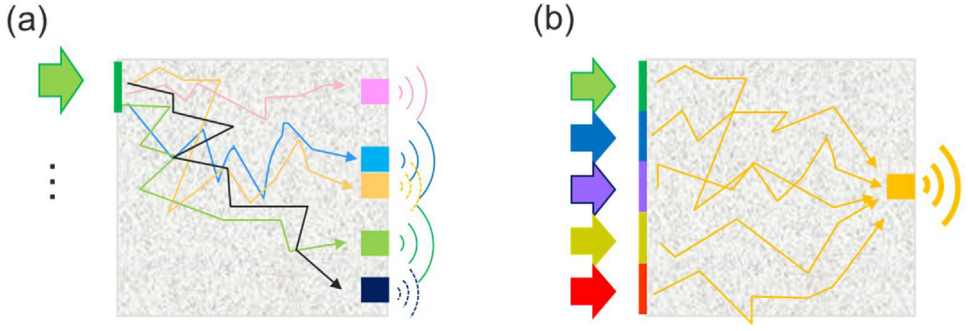

Fig. 1. Transmission matrix focusing through a scattering sample.
(a) Each incident light is scattered in the scattering sample, with each scattered light having a phase state different from that of the incident light state. The transmission matrix, the phase response of light, is simultaneously measured by either changing the whole area of each input light phase or encoding the illumination pattern and phase. (b) Optical wavefront shaping of the incident wave enables focusing light through the scattering sample with periodic phase matching by modulated incident light phase using the reverse phase of the transmission matrix.

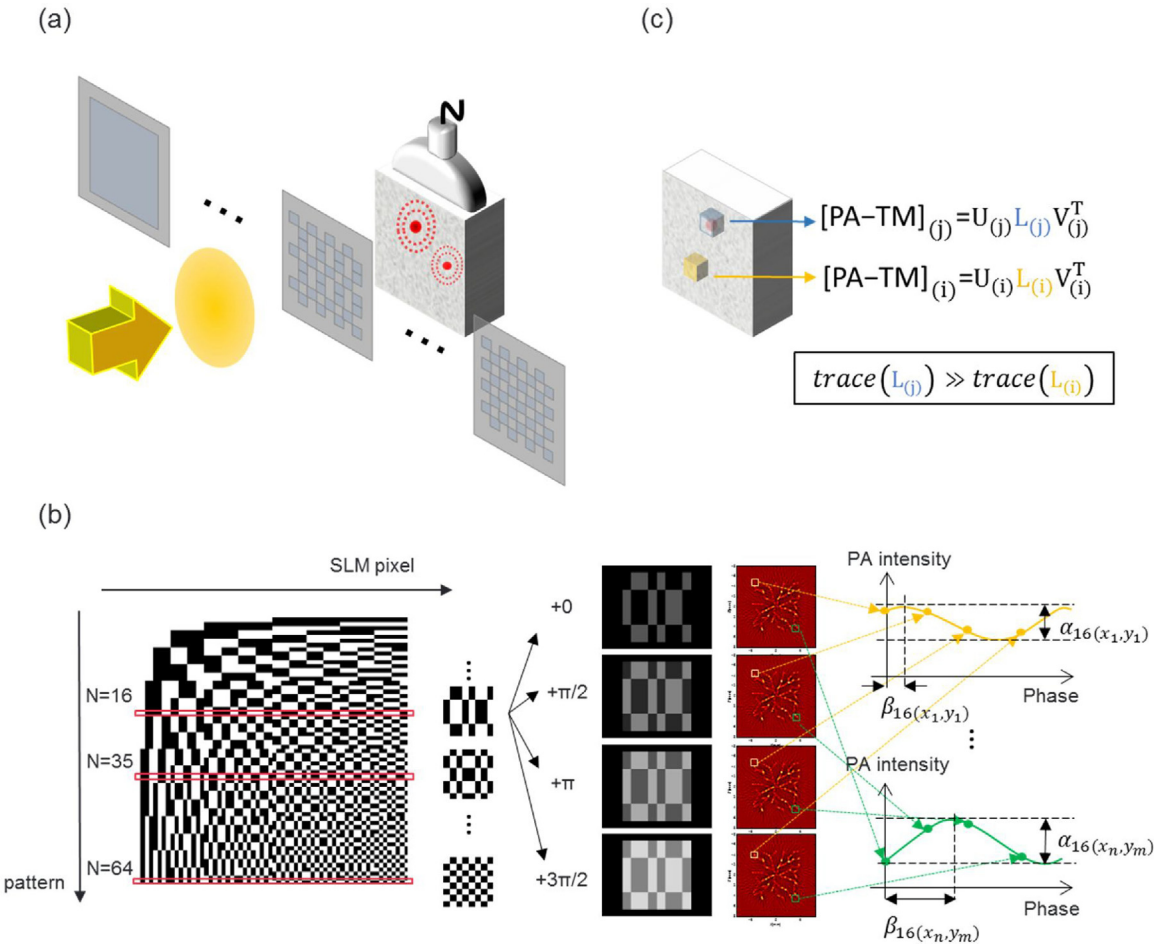

Fig. 2. Photoacoustic transmission matrix (PA-TM) through a scattering sample.
(a) Procedure for measuring the PA-TM: The incident light is modulated using a light modulation unit (e.g., SLM), and photoacoustic signals from the light-absorption targets are recorded by the transducers. The phase response of the light is simultaneously measured through photoacoustic signals by encoding the illumination pattern. The intensity modulation that reflects the phase response for each signal source is measured by reconstructing the photoacoustic signals detected for the illumination.
(b) The four phases for each Hadamard pattern (N = 8) are generated from the Hadamard matrix.
Each pattern is displayed on the SLM to shape the illuminating wavefront. The resulting photoacoustic signals are measured using a transducer, and the corresponding photoacoustic image is reconstructed for each phase step. The PA-TM is retrieved from this four-phase modulation for each image pixel area. The PA-TM is calculated from the 64 input Hadamard pattern response. The PA-TM is decomposed by singular values to obtain singular value vectors. The singular value photoacoustic image is calculated using the sum of the diagonal components of L (diagonal matrix), which is aligned to the image pixel.
(c) The phase response for light is expressed only where the light-absorbing body is present. Thus, the presence of the light-absorbing body can be identified by displaying the singular value image. The blue area ($[PA\text{-}TM]_i$), where there are light absorbers, has the response of the modulating light (L_i). This area enables enhancement or weakening of signals using light modulation. In contrast, the yellow area ($[PA\text{-}TM]_j$), which has no light absorbers, demonstrates no response of the modulating light (L_j).

Letting $|O|e^{\Phi o}$ be the scattered light to be modulated, the interference light with the reference light $|R|e^{\Phi R}$ can be expressed as

$$\begin{aligned} I &= |R+O|^2 = |R|^2 + |O|^2 + R^*O + RO^* \\ &= |R|^2 + |O|^2 + 2Re(R^*O) \\ &= |R|^2 + |O|^2 + 2|R||O|\cos(\phi + \delta\theta) \end{aligned} \quad (1)$$

Here, the response phase can be calculated using the phase-shift method by measuring $\delta\theta$ four times (0, π/2, π, and 3π/2) (Fig. 2 (b)).

$$\Phi_o = \arctan\left(\frac{I_{3\pi/2} - I_{\pi/2}}{I_0 - I_\pi}\right) \quad (2)$$

$$|O| = \sqrt{\frac{(I_0 - I_\pi)^2 + (I_{3\pi/2} - I_{\pi/2})^2}{4}} \quad (3)$$

The PA-TM is then calculated from the 64 input Hadamard pattern responses for each image pixel area ($\boldsymbol{x_n}, \boldsymbol{y_m}$), where $\boldsymbol{i}$ is the imaginary unit and $\mathbf{H}$ is the complex Hadamard matrix.

The response matrix (PA-TM) reconstructed with all Hadamard patterns is transformed into inputs for each modulation area by basis transformation as needed, and a PA-TM for each input phase of the smallest component unit of the Hadamard pattern is formed in each pixel. $\mathbf{H}^*$ is the Hermitian transpose of the complex Hadamard matrix.

$$\begin{aligned} \mathrm{PA-TM}_{(x_n,y_m)\boldsymbol{measured}} &= \mathbf{H} * \mathrm{PA-TM}_{(x_n,y_m)\boldsymbol{SLM-Hadamardinputbasis}} \\ &= \begin{bmatrix} |O|_{1(xn,ym)} e^{\Phi_{o\,1(xn,ym)} i} & \cdots & |O|_{57(xn,ym)} e^{\Phi_{o\,57(xn,ym)} i} \\ \vdots & \ddots & \vdots \\ |O|_{8(xn,ym)} e^{\Phi_{o\,8(xn,ym)} i} & \cdots & |O|_{64(xn,ym)} e^{\Phi_{o\,64(xn,ym)} i} \end{bmatrix} \end{aligned} \quad (4)$$

$$PA-TM_{(x_n,y_m)\boldsymbol{SLM-pixel\ \ input\ \ basis}} = \mathbf{H}^* * PA-TM_{(x_n,y_m)\boldsymbol{measured}} \quad (5)$$

It is then possible to decompose the phase-response matrix of each pixel into ULV^T (U, V: orthonormal matrix, L: diagonal matrix) using singular value decomposition, and to calculate the singular value, which is the diagonal component of L.

$$PA-TM_{(x_n,y_m)} = U_{(xn,ym)} L_{(xn,ym)} V^T_{(xn,ym)} \quad (6)$$

Here, the singular value is the response sensitivity for each light modulation area. It is possible to visualize the light-absorbing substance by displaying the response sensitivity for each pixel and displaying the presence/absence of the light response (Fig. 2(c)).

Once the PA-TM is calculated (5), the appropriate phase set for creating focus points is calculated sequentially [20]. Letting O^{focus} be the focusing point pattern, the input pattern I^{focus} can be expressed as

$$I^{focus} = \mathrm{PA} - \mathrm{TM}\dagger * O^{focus} / |PA - TM\dagger * O^{focus}| \quad (7)$$

where † is the conjugate transpose. The phase is then calculated from the phase angle of I^{focus}.

3. Simulation analysis

Fig. 3(a) illustrates the simulation system setup. Acoustic simulations were performed in two-dimensional (2D) space using a k-Wave toolbox [16]. In a simulation space with 1 μm pitch, we placed 200 μm transducers with bandwidths of 2 to 8 MHz in a 128-element 1D arrangement. As illustrated in Fig. 3(b), the light-absorbing body was a doughnut-shaped object with a 10 mm diameter, and its center was placed 15 mm from the transducers (at a depth of 15 mm). The irradiating light exhibited a speckled pattern in the scatterer and was generated based on random phase data [17]. The speckled pattern $S^{speckle}$ can be expressed as

$$S^{speckle} = IFFT\left(FFT\left(h(s) * e^{i\psi}\right)\right) \quad (8)$$

where $h(s)$ is the coherent transfer function, ψ is the added respective phase the initial input laser and the partitioned Hadamard patterns. Then the irradiating light forms a speckled pattern. We conducted an acoustic propagation simulation in which the reference light was shifted by four phases ($\pi/2$ interval), and different irradiation patterns reached the absorption body. We then reconstructed an image for 16×16 patterns $\times$ 4 phases based on acoustic propagation (Fig. 3(c)). The obtained response matrix gives a 16×16 transmission matrix for each reconstructed pixel. Fig. 3(e) indicates the singular value image for each pixel. For comparison, Fig. 3(d) presents the reconstructed image from acoustic propagation with normal, uniform illumination. For simulation with normal light, many signal components do not reach the transducers, giving rise to artefacts. In contrast, no artefacts are found in the singular value image, because signals that normally do not propagate are detected due to the response from the speckles. In particular, artefact areas are composed of the superposition of other multiple phase responses; consequently, no response corresponding to the singular value at that area can be obtained.

4. Experiment analysis

4.1. Materials and methods

Fig. 4(a) illustrates the experimental setup. A Ti:sapphire nanosecond pulse laser (LT-2111, LOTIS TII) pumped using a Q-switched Nd:YAG laser (LS-2137, LOTIS TII, 10 Hz pulse repetition frequency (PRF), 15 ns pulse width, 7 mm coherence length, and 20 mJ pulse energy at a wavelength of 800 nm) was used for the light source. Light fluctuation was monitored using a power meter (LabMAX-TO, coherent) and compensated for the detected photo-acoustic signal caused by the light fluctuation.

Phase modulation was performed using a phase-only SLM (X10468-02, 800×600 pixels, Hamamatsu Photonics K.K.). The SLM was connected to a PC via the DVI-D port. A laser beam was focused onto a ground glass diffuser (#240, Sigmakoki), and

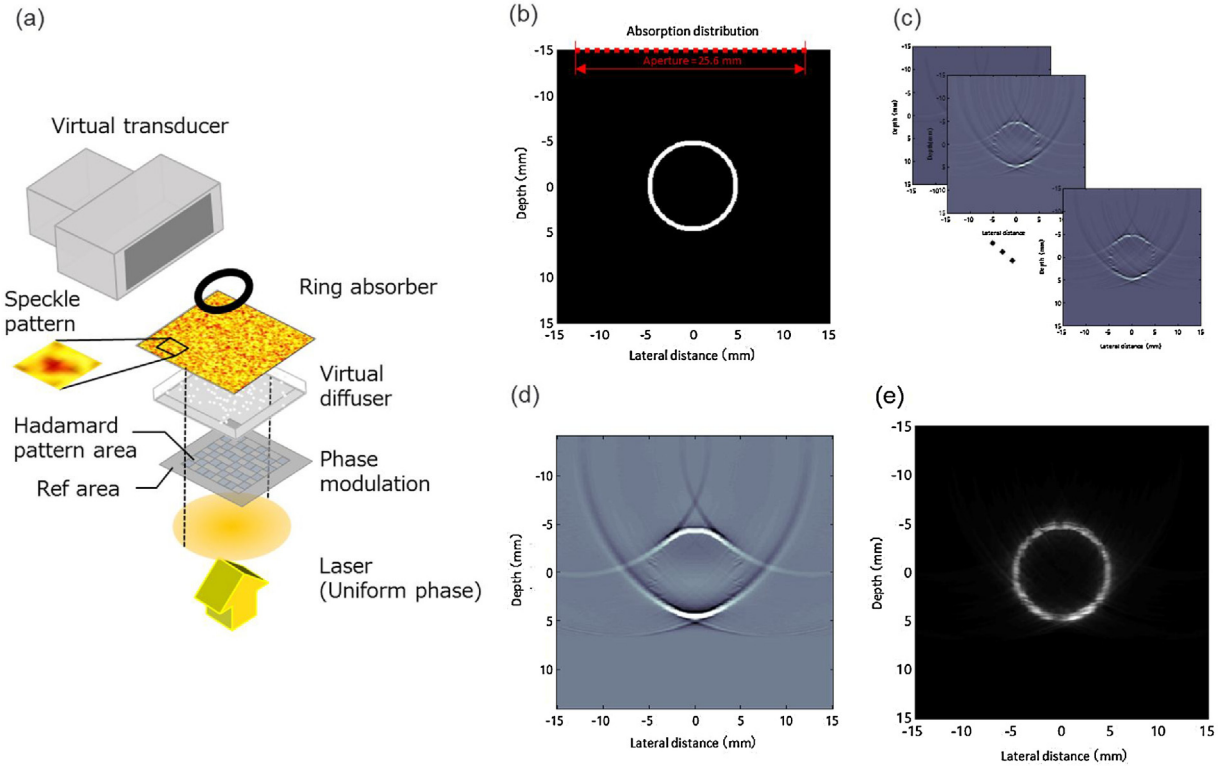

Fig. 3. Simulation results of a ring absorber illuminated with 16×16 Hadamard modulated light.
(a) Schematic of the simulation setting. Modulated scattering light was illuminated from the vertical side of an imaged plane. (b) Original absorption distribution. (c) Image reconstruction using conventional uniform illumination. (d) A plurality of illumination patterns encoded based on a Hadamard matrix. (e) Singular value image calculated using the transmission matrix of each pixel.

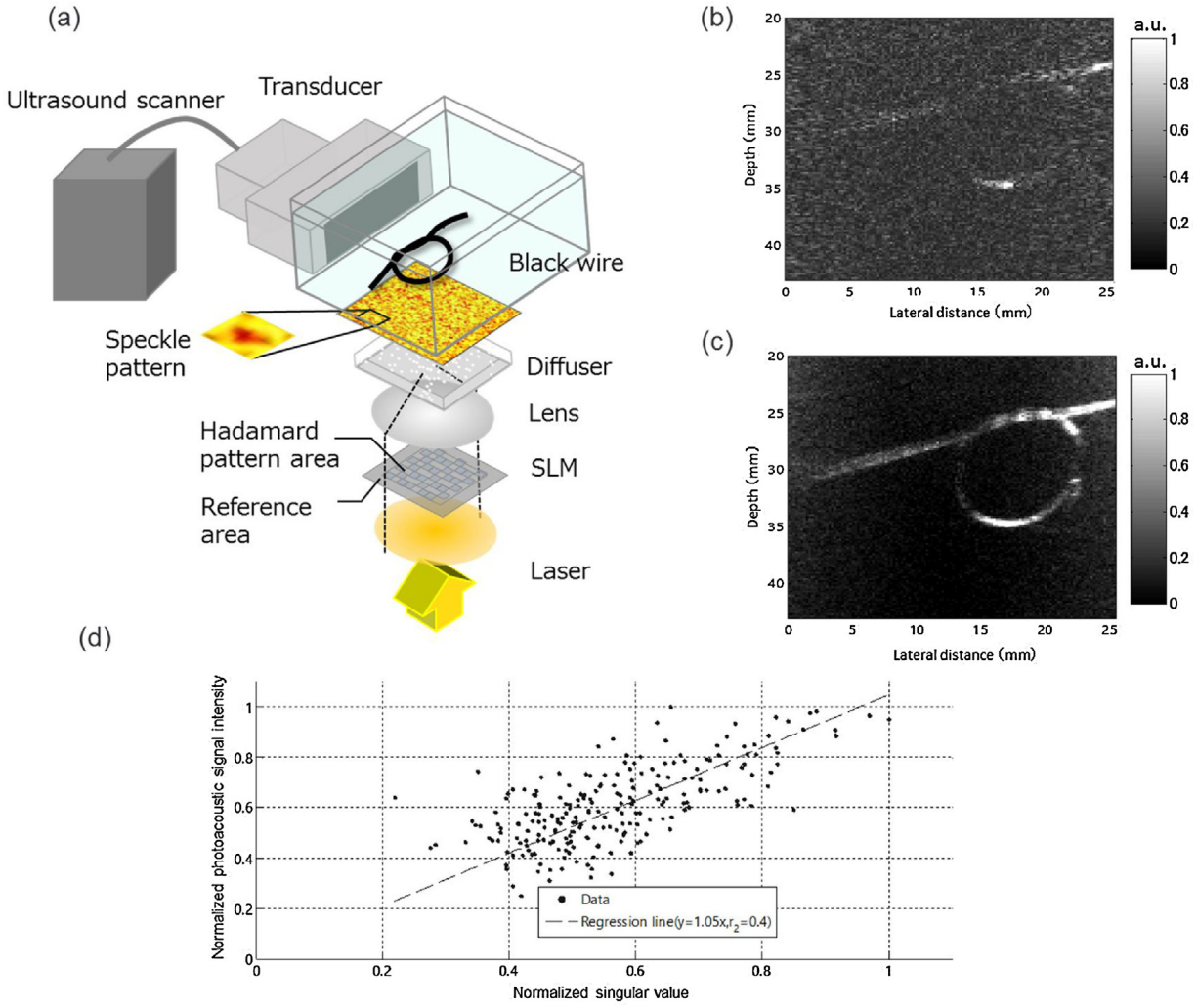

Fig. 4. Experiment results of a wire phantom illuminated with 8×8 Hadamard modulated light.
(a) System schematic. The signal acquisition system used a commercial ultrasound system and a 1D ultrasound probe. (b) Average photoacoustic-computed tomography image from all modulated raw signal data. (c) Singular value image calculated using each PA-TM. (d) Scatter plot and linear approximation of the relationship between the normalized image signal intensity resulting from increased photoacoustic signal intensity and the normalized singular value found at each point.

speckle illumination reached the gelatine phantom including the light-absorbing substance to generate a photoacoustic wave.

The photoacoustic image was detected using a general ultrasound imaging system (Aixplorer, Supersonic Imagine) with a 192-element linear array (SL15-4; bandwidth 4 to 15 MHz). Data was detected iteratively, and the photoacoustic image was used to calculate the transmission matrix and singular value using a PC running MATLAB (MathWorks, Inc.).

A delay generator (DG645, Stanford Research) was used as the master clock for the system. The delay generator sent triggers to the Q-switched laser and power meter systems.

The phantom consisted of 2% agar injected into a 500 μm-diameter carbon wire in the middle of the phantom (20 mm thick). Polymethylmethacrylate fine particle (Techpolymer, MBX-40, Sekisui Plastics Co., Ltd.) of 3% was used for the ultrasonic waver scatterer.

4.2. Acquisition procedure

The shaped laser beam was used to irradiate an SLM that was split into 8×8 phase-controlled block segments (1 block segment = 60×60 pixels), each with a 0 or π phase Hadamard matrix pattern, and the rest of the pixels were used for the reference phase area for the four-phase (0, $\pi/2$, π, and $3\pi/2$) shift. Sixty-four patterns of Hadamard matrix illumination were then displayed on the SLM for each of the four reference phases. The total measurement time was 25.6 s. The ultrasound system sequentially detected the photoacoustic signals emitted from the light-absorption target.

After all signals were obtained, a photoacoustic image was reconstructed using the universal back projection algorithm [18] with a pixel space of 0.2 mm. Next, 64 patterns of the Hadamard matrix phase response were calculated using the four-phase shift. A singular value image was then calculated using the PA-TM.

4.3. Experiment results

We analysed the experiment results obtained from a phantom and prepared a light source with a modulated scattering status and illuminated the phantom from the side (Fig. 4(a)). The knotted rubber wire in the gelatine absorbs light and propagates photoacoustic waves, which are detected by an ultrasound probe located on the top of the phantom. Fig. 4(b) presents the image obtained from integrating the sequence data, and Fig. 4(c) presents the singular value image. This singular value image depicts the linear shape of the vertical component from the transducers, which is

normally difficult to extract. In the integrated image, the noise components are scattered on a background image other than the light-absorbing body, while such components are not present in the singular value image. This is likely because the random noise component is cancelled in the phase calculation. Therefore, this method verifies the validity of this measurement in environments with a low signal-to-noise ratio.

For the location identified as the light-absorbing body, we constructed a target-specific focusing function that imparts a higher light intensity to pixels in that location than in other regions, and derived the phase map from the PA-TM. Fig. 4(d) plots the reconstructed increased intensity and the singular value at each point obtained. Despite the apparent dispersion, it confirms that the singular value image represents the light-phase response in the plane.

5. Discussion

Our method solved two problems in 1D probe measurement systems. First, it regulated the omission of image components under limited view by treating light as speckles. Second, the reconstruction artefacts in the non-signal region were regulated, and the SNR was improved by calculating the response for each reconstruction pixel region. In contrast, J Gateau et al. [14,15] proposed the Gini mean difference image technique to receive the photoacoustic wave, using the speckled illumination as the point spread propagated wave to overcome limited view. The demonstration experiment results for the Gini mean difference image and singular value image are compared (Fig. 5). This measurement uses the agar phantom with ultrasonic scattering materials that located two wires almost in parallel (Fig. 5(a)). The Gini mean difference image from all modulated raw signal data for the PA-TM is presented in Fig. 5(b). A foggy noise is confirmed behind the wires. In contrast, for the singular value image in Fig. 5(c), the foggy noise is substantially unobserved at the wires. Comparison of the two methods indicates few differences in the imaging of the light absorbers. However, a key advantage of the singular value image is that scattering artefacts are almost never observed. The scattering artefact is generated by the photoacoustic signal of the light absorbers, via acoustic backscattering at echogenic structures inside the living body (e.g., the muscle layer or fatty layer). These scattering artefacts, where there is no light absorber, are made of the many scattering photoacoustic signals from the many light absorbers, and do not give a sharp image because of the lack of consideration of changing the time of flight after scattering in image reconstruction. In this case, the Gini mean image has some values because the reconstructed image made of the scattering photoacoustic signal itself is measured. However, PA-TM singular value relatively shows a low value because the mismatch of each phases from the signals of the other points in comparison with the point consisting of the single phase response of the corresponding light absorber. Thus, a singular value image having a high contrast between the presence and absence of light absorbers is available.

In this study, we used the Hadamard matrix to measure the phase response of the light. This matrix can quickly transform the signal for the entire visualization region into the response. The simultaneous modulation of measurement space data contributes to shorter measurement times. Although the measurement time is sufficiently shorter than that for point-wise data measurement [19], it is necessary to complete the measurements in less than the correlation time in light when applying this method to dynamic objects such as living bodies [21]. The current time is restricted by the laser PRF. It is possible to speed up the process by changing to a high PRF laser and replacing the SLM with a magneto-optic SLM or a digital micromirror device [22].

The central frequency band of the photoacoustic signal changes in proportion to speckle size when the speckle is smaller than the light-absorbing body. Therefore, a probe should be designed to detect signals corresponding to the small speckle of light generated in the light scatterer. If the measured object is as small as the speckle (e.g., blood vessels), probes that can detect corresponding high frequencies are needed. This is presumably the reason for the derivation of a small singular value for the vertical components of the probe (Fig. 4(c)) and indicates the need for optimizing the system to correspond with the target configuration. Although it is difficult to correctly ascertain the speckle size in the scatterer of the phantom, since the lateral direction is emphasized, it is presumed that the current speckle size is 300 μm or more, slightly larger than the diameter of the wire. In order to observe with equal intensity as in the simulation in both the longitudinal and lateral directions, it is preferable that the speckle size is equal to or less than the diameter of the wire. Furthermore, it is preferable to use a

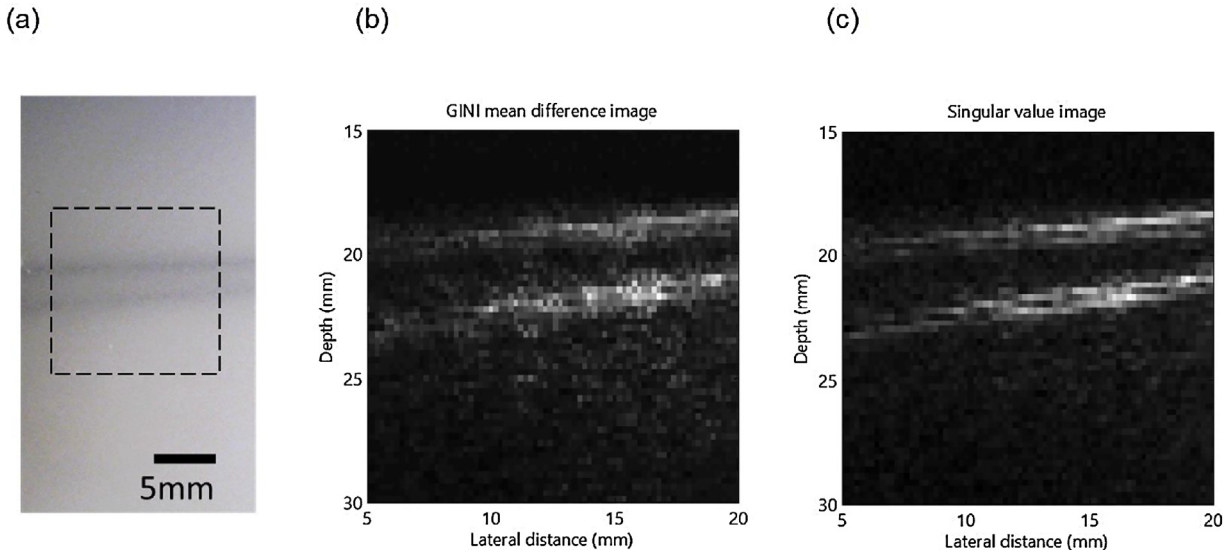

Fig. 5. Comparative experiment results for the Gini mean difference image and the singular value image.
(a) Photograph of a phantom at the location of the imaging plane. Two wires are arranged almost in parallel inside an agar phantom including ultrasonic scattering materials. The image-forming region is a dashed line area. (b) Gini mean difference image from all modulated raw signal data. (c) Singular value image calculated using each PA-TM.

probe at the center frequency of 5 MHz corresponding to the bandwidth generated from a blood vessel of 300 μm in order to clearly depict a blood vessel image like this wire diameter. Nonetheless, this system provides a quantitative representation of the light response (Fig. 4(d)) and thereby enables more effective clarification within the derived region than other systems. Forming the light-energy distribution in the desired region and shape after PA-TM derivation, as described above, this TM method demonstrated greater efficacy in intensity enhancement than methods that observe phase difference by scanning the signal point-by-point [19]. Using the time of flight from the desired region, this system could compensate the dispersion of the speed of sound in the reconstruction process in an in vivo or ex vivo environment, which merits further research. However, there is no current data on the sensitivity of this system with respect to biometric measurement, and we would like to make it a future task.

Meanwhile, when the speckle number for light related to modulation within the observed object (light-absorbing body) increases, it is more difficult to observe modulation in the target region (image pixel size), as with time-reversed ultrasonically encoded optical focusing [9,23]. However, the purpose of the transmission matrix in this method is not to focus the light. Therefore, it can be applied for signals from deeper regions in the sense that it can be used to visualize light-absorbing bodies even in the minute modulation region with no focus effect.

Another point is that speckle uses the behaviour of coherent light. However, coherence is lost in deeper regions, and measurement using this method is difficult. Despite these future challenges, the use of lasers with high coherence is essential to ensure coherence. Possible solutions to the increased number of speckles include a method that uses nonlinearity based on photoacoustic measurement principles to decrease the density of photoacoustic signals generated during measurement [24]. With any method, measurement with a high SNR for deeper parts is possible by combining the merits of this measurement method in high-scattering regions and the focusing of light using the PA-TM. A breakthrough in photoacoustic measurement is expected by adding roles such as light enhancement, locality of space, and correction of lost signals to the conventional role of light, which is the propagation of energy.

Conflict of interest

The authors declare that there are no conflicts of interest.

References

[1] Yuan Xu, Lihong V. Wang, Reconstructions in limited-view thermoacoustic tomography, Med. Phys. 31 (April (4)) (2004).
[2] Andreas Buehler, Marcin Kacprowicz, Adrian Taruttis, Vasilis Ntziachristos, Real-time handheld multispectral optoacoustic imaging, Opt. Lett. 38 (May (9)) (2013) 1.
[3] X. Luís Deán-Ben, Daniel Razansky, Portable spherical array probe for volumetric real-time optoacoustic imaging at centimeterscale depths, Opt. Express 21 (23) (2013) 28071.
[4] Michael Jaeger, Jeffrey C. Bamber, Martin Frenz, Clutter elimination for deep clinical optoacoustic imaging using localised vibration tagging (LOVIT), Photoacoustics 1 (2013) 19–29.
[5] Puxiang Lai, Xiao Xu, Honglin Liu, Lihong Wang, Time-reversed ultrasonically encoded optical focusing in biological tissue, J. Biomed. Opt. 17 (March (3)) (2012).
[6] Ke Si, Reto Fiolka, Meng Cui, Fluorescence imaging beyond the ballistic regime by ultrasound-pulse-guided digital phase conjugation, Nat. Photonics 6 (2012).
[7] Ying Min Wang, Benjamin Judkewitz, Charles A. DiMarzio, Changhuei Yang, Deep-tissue focal fluorescence imaging with digitally time-reversed ultrasound-encoded lightNature, Communications 3 (2012) (Article number: 928).
[8] M. Cui, C. Yang, Implementation of a digital optical phase conjugation system and its application to study the robustness of turbidity surpression by phase conjugation, Opt. Express 18 (2010) 3444–3455.
[9] Yuta Suzuki, Jian wei tay, qiang yang, lihong wang, digital reflection-mode time-reversed ultrasonically encoded (TRUE) optical focusing, Proc. SPIE 8943 (2014) (89431B).
[10] I.M. Vellekoop, A.P. Mosk, Focusing coherent light through opaque strongly scattering media, Opt. Lett. 32 (16) (2007) 2309–2311.
[11] Donald B. Conkey, Albert N. Brown, Antonio M. Caravaca-Aguirre, Rafael Piestun, Genetic algorithm optimization for focusing through turbid media in noisy environments, Opt. Express 20 (5) (2012) 4840–4849.
[12] Fanting Kong, Ronald H. Silverman, Liping Liu, Parag V. Chitnis, Kotik K. Lee, Y. C. Chen, Photoacoustic-guided convergence of light through optically diffusive, Media Opt. Lett. 36 (11) (2011) 2053–2055.
[13] T. Chaigne, O. Katz, A.C. Boccara, M. Fink, E. Bossy, S. Gigan, Controlling light in scattering media non-invasively using the photoacoustic transmission matrix, Nat. Photonics 8 (2014).
[14] J. Gateau, T. Chaigne, O. Katz, S. Gigan, E. Bossy, Improving visibility in photoacoustic imaging using dynamic speckle illumination, Opt. Lett. 38 (23) (2016) 5188–5191.
[15] Thomas Chaigne, Jérôme Gateau, Ori Katz, Emmanuel Bossy, Sylvain Gigan, Light focusing and two-dimensional imaging through scattering media using the photoacoustic transmission matrix with an ultrasound array, Phy. Opt. 39 (9) (2014) 2664–2667.
[16] B.E. Treeby, B.T. Cox, k-Wave: MATLAB toolbox for the simulation and reconstruction of photoacoustic wave-fields, J. Biomed. Opt. 15 (2) (2016) 021314.
[17] Sébastien Equis, Pierre Jacquot, Simulation of speckle complex amplitude: advocating the linear model, Proc. SPIE 6341 (2006) 634138 (Speckle06: Speckles, From Grains to Flowers).
[18] Minghua Xu, Lihong V. Wang, Universal back-projection algorithm for photoacoustic computed tomography, Phys. Rev. E 71 (2005) 016706.
[19] Donald B. Conkey, Antonio M. Caravaca-Aguirre, Jake D. Dove, Hengyi Ju, Todd W. Murray, Rafael Piestun, Super-resolution photoacoustic imaging through a scattering wall, Nat. Commun. 6 (2015) 7902.
[20] S.M. Popoff, G. Lerosey, R. Carminati, M. Fink, A.C. Boccara, S. Gigan, Measuring the transmission matrix in optics: an approach to the study and control of light propagation in disordered media, Phys. Rev. Lett. 104 (2010) 100601 (Published 8 March).
[21] Joshua Brake, Mooseok Jang, Changhuei Yang, Analyzing the relationship between decorrelation time and tissue thickness in acute rat brain slices using multispeckle diffusing wave spectroscopy, J. Opt. Soc. Am. A 33 (2) (2016).
[22] Jian Wei Tay, Jinyang Liang, Lihong V. Wang, Amplitude-masked photoacoustic wavefront shaping and application in flowmetry, Opt. Lett. 39 (19) (2014).
[23] Yan Liu, Puxiang Lai, Cheng Ma, Xiao Xu, Alexander A. Grabar, Lihong V. Wang, Optical focusing deep inside dynamic scattering media with near-infrared time-reversed ultrasonically encoded (TRUE) light, Nat. Commun. 6 (2015) 5904.
[24] Puxiang Lai, Lidai Wang, Jian Wei Tay, Lihong V. Wang, Photoacoustically guided wavefront shaping for enhanced optical focusing in scattering media, Nat. Photonics 9 (2015) 126–132.

Hiroshi Abe. Hiroshi Abe is a PhD student in the Department of Human Health Sciences, Graduate School of Medicine, Kyoto University. He received his B.S. and M. S. degrees in Electrical and Electronic Engineering from the Kyushu University. He has been working for Canon Inc. since 2007 as a Research Engineer. His major research interests are the development of optoacoustic systems for breast cancer and other clinical applications.

Tsuyoshi Shiina. Dr. Shiina was graduated from the Electronic Engineering Department, the University of Tokyo, in 1982. He received PhD degrees in electronic engineering in 1987 from the University of Tokyo. He also received DMSC degree in 2006, from University of Tsukuba. From 1995 to 1996, he was with the institute of Cancer Research and the Royal Marsden NHS Trust in UK as Visiting Professor. He has been a Professor of Graduate School of Systems and Information Engineering, the University of Tsukuba since 2001. He is presently a Professor of Human Health Sciences, Graduate School of Medicine, Kyoto University since 2008. He also served as a Deputy Director of Kyoto University Hospital from 2012 to 2015. His current research interests include visualization technique of structural and functional bio-information, for example, ultrasonic elasticity imaging and photoacoustic imaging. Recently, he involves the development of photoacoustic mammography as Kyoto University-Canon joint research project and the ImPACT program supported by Japanese government grant. He is vice-president of the Japan Society of Ultrasonics in Medicine (JSUM) from 2014. Hiroshi Abe. Tsuyoshi Shiina